Published in final edited form as:

Proteins. 2022 November ; 90(11): 1987–2000. doi:10.1002/prot.26391.

Oxidation of active cysteines mediates protein aggregation of S10R, the cataract-associated mutant of mouse GammaB-crystallin

Wenjuan Hou[1,2,3], **Ajay Pande**[1], **Jayanti Pande**[1]

[1]Department of Chemistry, Life Sciences, University at Albany, State University of New York, Albany, NY, USA

[2]Current address: BioLegend Inc., 8999 BioLegend Way, San Diego, CA 92121, United States

Abstract

The Ser10 to Arg mutation in mouse γB-crystallin has been associated with protein aggregation, dense nuclear opacity and the degeneration of fiber cells in the lens core. Overexpression of the gap junction protein, connexin 46, was found to suppress the nuclear opacity and restore normal cell-cell contact[1,2]. However, the molecular basis for the protein aggregation and related downstream effects, were not evident from these studies. Here we provide a comparison of the structures and solution properties of wild-type mouse γB-crystallin and the S10R mutant *in vitro*, and show that, even though the mutation does not directly involve cysteine residues, some cysteines in the mutant protein are activated, leading to the enhanced formation of intermolecular disulfide-crosslinked protein aggregates relative to the wild-type. This occurs even as the protein structure is essentially unaltered. Thus, the primary event is enhanced protein aggregation due to the disulfide crosslinking of the mutant protein. We suggest that these aggregates eventually get deposited on fiber cell membranes. Since the gap junction protein, connexin 46 (Cx46) is involved in the transport of reduced glutathione, we posit that these deposits interfere in Cx46-mediated glutathione transport and facilitate the oxidative stress-mediated downstream changes. Overexpression of Cx46 suppresses such oxidative aggregation. These studies provide a plausible explanation for the protein aggregation and other changes that accompany this mutation. If indeed cysteine oxidation is the primary event for protein aggregation also *in vivo*, then the S10R mutant mouse, which is currently available, could serve as a viable animal model for human age-onset cataract.

---

[3]This work was accepted as a poster presentation at the annual meeting of the Association for Research in Vision and Ophthalmology, 2020, Baltimore, MD. It constitutes a part of the PhD thesis of W.H. at the University at Albany, State University of New York.

CORRESPONDENCE: Jayanti Pande, Department of Chemistry, Life Sciences 2076, University at Albany, State University of New York, 1400 Washington Avenue, Albany, NY 12222, jpande@albany.edu.

AUTHOR CONTRIBUTIONS

WH performed all the experiments, analyzed the data and wrote the experimental section, AP contributed to designing the study and writing the manuscript, made the MGB and S10R cDNA constructs, and carried out molecular modeling and bioinformatics analysis, JP contributed to designing the study and writing and editing the manuscript.

ETHICS STATEMENT

This work was conducted under the strict ethical standards set by the University at Albany, State University of New York.

CONFLICT OF INTEREST

None

Keywords

Mouse γ-crystallin; cysteine activation; thiol oxidation; hydrophobicity; connexin 46

1. INTRODUCTION

In 2008, Li et al.[1] reported a mutant mouse with a dense nuclear cataract that they identified as a Ser11 to Arg or S11R[†] mutation in the γB-crystallin gene. This is a dominant mutation that shows 100% penetrance. Dense deposits of mutant γB-crystallin were observed in the inner fiber cells, while the peripheral layers were normal. Homozygous lenses showed a dense nuclear opacity while the heterozygous lenses showed only a hazy nuclear region. Observation of a dense nucleus correlated with an increase in calcium, cleavage of crystallins and their aggregation. These observations led the authors to suggest that the mutation causes the mutant protein to aggregate, and is accompanied by an increase in calcium concentration, triggering of proteases like the calpains leading to the cleavage of crystallins, and the degeneration of fiber cells in the lens core.

In a subsequent report these authors[2] further showed that the fiber-to-fiber contacts in mature fiber cells were severely disrupted in the homozygous mice. More importantly, in compound homozygous mutant mice (i.e., those with homozygous α3-connexin (Cx46) knock-in), the nuclear cataract was suppressed and near-normal cell-cell contact restored. Along with the restoration of lens transparency and levels of calcium, the integrities of the crystallins and fiber cells were also restored. Clearly, the overexpression of Cx46 *somehow* seemed to mitigate the deleterious effects due to the S11R[†] mutation in γB-crystallin. These studies led to the hypothesis[2] that this mutation results in protein aggregation, cytoskeletal damage, and increased calcium concentration, and the overexpression of Cx46 – a gap-junction protein – normalizes calcium concentration and restores transparency.

Reviewing the literature for γ–crystallin mutations, readily shows that in several cataract-associated mutations in human γ–crystallins, Arg residues are substituted with a Ser. However, there are no prior reports of opposite cases— namely the replacement of a Ser by an Arg, in human or mouse γ–crystallins (cat-map.wustl.edu). This apparent anomaly raised the question as to how the substitution of a polar but uncharged Ser residue with a polar and charged residue like Arg could lead – counterintuitively – to protein aggregation? Even more intriguing was the observation of Li et al[2] that overexpression of Cx46 almost totally mitigated the effect of mutation, and restored lens transparency. These puzzling questions prompted us to examine the S10R mutation further. The results of those studies are presented here.

To examine the effect of replacing a Ser with an Arg, we expressed both proteins — i.e. wild-type recombinant mouse γB-crystallin (MGB), and its S10R mutant (S10R[†]), and compared their solution properties under a defined set of experimental conditions. The data

[†]The notation S11R[1] refers to the Serine mutation at position 11 in the γB-crystallin gene, counting the N-terminal methionine[1,2]. For expressed proteins, the first Met is omitted, and the mutation is referred to as S10R, which is the notation used throughout this report.

show that replacement of Ser10 with an Arg activates some Cys residues in the S10R mutant, even though the mutation by itself does not directly involve Cys residues. Such replacement facilitates disulfide-crosslinked protein aggregation under oxidizing conditions in solution, relative to MGB. A bioinformatic analysis of MGB and S10R points to the involvement of multiple Cys residues in protein aggregation. These observations led us to suggest that – in the lens – overexpression of the gap junction protein Cx46, reverses much of the Cys-mediated protein aggregation and related, damaging downstream effects observed by these authors, because Cx46 enables the transport of reduced glutathione (GSH) to the lens nucleus[3].

2. MATERIALS AND METHODS

2.1 Protein expression and purification

cDNA construct for MGB and S10R: Starting from the plasmid for bovine γB-crystallin[4] (BGB), mutations were made using the Quickchange Multi Site-Directed Mutagenesis kit (Agilent) and the appropriate primers, to produce the plasmid for mouse γB-crystallin. The following primers and their reverse complements were used in producing the cDNA construct for MGB and S10R from the BGB construct. As intermediate constructs appeared important for other investigations, we chose to undertake the lengthy process of stepwise mutations, instead of synthesizing the cDNA construct of interest directly. Listed below are the amino acid substitutions, and the corresponding primers used to transform the BGB construct.

For Y6F, G10R, & H14R

5’-3’: C ACT TTT TTC GAG GAC CGG CGC TTC CAG GGC CGC TGC TAC G

For P27T & I35V

5’-3’: CCC AAC CTG CAG ACC TAT TTC AGC CGC TGT AAC TCC GTC CGC G

For D61E & N72S

5’-3’: GC GAG TAC CCC GAC TAC CAG CAG TGG ATG GGC TTC AGC GAC TCC

For T85S & F88Y

5’-3’: C CCG CAA CAC AGC GGC ACT TAC AGA ATG AG

For R95K

5’-3’: G AGA ATC TAT GAG AAA GAT GAC TTC AGA GGA CAG ATG

For P110L

5’-3’: G ATC ACA GAC GAT TGT CTC TCT CTT CAA GAC CGC

For L118F, T119S & V121I

5’-3’: CAA GAC CGC TTC CAC TTC TCT GAG ATT CAC TCC CTC

For L127M & S130C

5’-3’: CC CTT AAC GTG ATG GAG GGT TGC TGGGTC C

For M160A & L167F

5’-3’: GG GGG GCA GCG AAT GCC AAA GTT GGTTCT TTC AGA CGG G

For R79C

5’-3’: CCA TCC GCT CCT GCT GCC TCA TCC CGC

For G10S (i.e. WT-MGB)

5’-3’: C GAG GAC CGG AGC TTC CAG GGC C

Mutations were confirmed with sequence analysis by Eurofins Genomics. Protein expression and purification were carried out as described below.

Procedures for protein expression and purification were almost identical to those used for human γD-crystallin[5]. Briefly, *E coli* (BL21 (DE3)) cells were grown at 37°C to an absorbance of ~0.7. The protein of interest was overexpressed by induction with isopropyl β-D-1-thiogalactopyranoside (IPTG) at a final concentration of 1 mM. Cell pellets were lysed in a buffer containing 5 mM Tris–HCl, pH 8, 25 mM NaCl, 2 mM EDTA, 1 tablet protease inhibitor (Complete, Roche biochemical), and lysozyme (250 μg/mL). Cells were lysed using five cycles of a rapid freeze-thaw procedure, by rapid freezing in liquid nitrogen and thawing in water at 30°C. The lysate was incubated with 25 μg/mL DNase (Sigma) followed by centrifugation at 48,000×*g*, to collect the supernatant. The supernatant and pellet were tested for the presence of crystallins by using SDS-PAGE. Both MGB and S10R crystallins fractionated almost exclusively (>95%) into the supernatant.

Protein purification was carried out in two steps, first using size-exclusion chromatography, followed by cation-exchange chromatography according to established procedures[6]. Electrospray Ionization Mass Spectroscopy (ESI-MS) analysis was performed as a criterion of purity, using an Agilent 6500 series Q-TOF LC/MS System, with a Halo 1000Å C4 column. All molecular weights (MWs) determined by ESI-MS are consistent with the “theoretical” MWs computed from the protein sequences (www.expasy.ch). Protein concentrations were determined from the absorbance at 280 nm using molar extinction coefficients obtained from Expasy (www.expasy.ch) (Table 1).

2.2 Gel electrophoresis and protein quantification

SDS–PAGE analyses were performed on a Bio-Rad Mini-Protean-II gel electrophoresis system, using 12–15% polyacrylamide gels under reducing and non-reducing conditions, according to the protocols provided in the Bio-Rad manuals. Isoelectric focusing (IEF) runs were made on a model 111 mini IEF apparatus from Bio-Rad. Coomassie Blue R-250 dye and crocein scarlet were used to detect the protein bands.

2.3 Circular Dichroism and Fluorescence spectroscopy

Circular Dichroism (CD) spectra were recorded on a JASCO J-815 spectropolarimeter. Near-UV CD spectra were measured using protein concentrations of 1 mg/mL in 100 mM sodium phosphate buffer (pH 7.1) in a 10 mm path length cuvette. Far-UV CD spectra were

measured using protein concentrations of 0.1 mg/mL in 10 mM sodium phosphate buffer (pH 7.1) in a 1 mm path length cuvette. All CD measurements were collected at room temperature using a bandwidth of 1.0 nm, a step interval of 1 nm, and a scanning speed of 50 nm/min (near-UV) or 100 nm/min (far-UV). Each CD spectrum was an average of nine scans. All spectra were normalized with respect to protein concentration.

Tryptophan fluorescence spectra were recorded on a Horiba Jobin Yvon Fluorolog-3 spectrofluorometer using excitation at 295 nm. Emission spectra were recorded from 305 nm to 450 nm with both slits set to 5 nm. Protein samples at 0.1 mg/mL were prepared in 100 mM sodium phosphate buffer (pH 7.1).

2.4 Quantification of the thiol groups in MGB and S10R

Solutions of MGB and S10R were first reduced with 5 mM TCEP (tris (2-carboxyethyl) phosphine) for 10 min, and the extra TCEP was washed out thoroughly with multiple aliquots of 100 mM sodium phosphate buffer (pH 7.1) followed by centrifugation using Amicon 10K cutoff filters. DTNB (5, 5'-dithio-bis-(2-nitrobenzoic acid) assays were performed under native and unfolded conditions for both proteins. Reduced proteins at a concentration of 0.1 mg/mL (5 μM) were added to a 1 mM DTNB solution with or without 6M GuHCl (guanidine hydrochloride) and incubated for 1 hr. Absorbance at 412 nm was measured as a function of time after the addition of DTNB. The molar extinction coefficients of the TNB^{2-} (2-nitro-5-thiobenzoic acid) moiety at 412 nm (14,150 $M^{-1}cm^{-1}$ in 0.1 M phosphate buffer without GuHCl, and 13,700 M^{-1} cm^{-1} in buffered 6M GuHCl) were used to estimate the number of free thiols in the unfolded and folded states respectively[7] for both proteins. For each experiment, three replicates were carried out.

2.5 Effect of biological and non-biological oxidants on protein aggregation

Reactions with each oxidant were carried out in triplicate and the values reported are the average of the three runs.

Reaction with H_2O_2: To monitor H_2O_2-induced protein aggregation profiles, DTT-reduced MGB and S10R samples (20 μM) were incubated with 10 mM H_2O_2 in 100 mM Tris-HCl buffer (pH 8.5) at 37°C. Absorbance at 360 nm was measured as a function of time after the addition of H_2O_2. To check protein aggregation rates, samples withdrawn at different time intervals were spun down and protein concentrations were measured in the supernatants.

Reaction with oxidized glutathione (GSSG): To monitor GSSG-induced protein aggregation profiles, DTT-reduced MGB and S10R samples (20 μM) were incubated with 15 mM GSSG in 100 mM Tris-HCl buffer (pH 8.5) at 37°C. Absorbance at 360 nm was measured as a function of time after the addition of GSSG. To check protein aggregation rates, samples withdrawn at 1 hr intervals were spun down and protein concentrations were measured in the supernatants.

Reaction with diamide: To monitor diamide-induced protein aggregation profiles, DTT-reduced MGB and S10R samples (40 μM) were reacted with 1 mM diamide in 100 mM

sodium phosphate buffer (pH 7.1) at 37°C. Absorbance at 400 nm was measured as a function of time after the addition of diamide. To check protein aggregation rates, samples withdrawn at 1 hr intervals were spun down and protein concentrations were measured in the supernatants.

2.6 Protein modeling and bioinformatics

To date, the 3D structure of MGB is not known, although the high-resolution x-ray crystal and solution NMR structures of several γ–crystallins have been determined. Therefore we modeled the structures of MGB and S10R by homology modeling using the Phyre2 server[8] for a quick assessment of the structures. For the more detailed analysis presented here, we used the "best model or model 1" automatically-generated by the I-TASSER server[9]. I-Tasser (or Zhang-server) uses an elaborate multiple template-based structure prediction. The templates used in this case had at least a 1.7Å resolution and better than 80% homology to the target proteins (WT or S10R mutant). This gives us confidence in the accuracy of these protein models. Our discussion of these proteins, and the reactivity of cysteines, is based on these models. Accessibility values for the cysteines were determined using the program NACCESS[10]. Cysteine pK_a values were determined using the CPIPE[11], DelPhiPK_a[12], and H^{++} [13] servers.

To depict the predominantly hydrophobic regions as well as the acidic and basic charged groups in Fig. 8, we used the highlighting scheme YRB proposed and implemented for Pymol software by Hagemans et al.[14].

3. RESULTS

3.1 Mouse γB-crystallin and its S10R mutant have nearly identical solution structures

MGB and S10R were expressed, purified and characterized by gel electrophoresis and spectral methods. As shown in the IEF gel in Fig. 1, the pI values for MGB and S10R are 7.05 and 7.3 respectively. The pI of WT-MGB found experimentally is identical to the expected value (web.expasy.org/protparam/). Thus, MGB at pH 7 is close to its isoelectric point and would normally be expected to show minimum solubility. The computed pI of the S10R mutant, using web.expasy.org/protparam/ is ~ 7.6. Therefore, a Ser to Arg mutation (or vice-versa), should result in a change of pI of about 0.6 pH units. This is the case, for example, for the R76S mutation in human γD-crystallin (HGD[15]), in which the replacement of Arg76 with a Ser lowers the pI of the mutant to 6.8 from 7.4 in WT-HGD. However, for the S10R mutation, we observe an increase of only about 0.3 pH units, suggesting that the positive charge in Arg10 is not fully realized and that Arg10 may be involved in additional interactions.

With regard to their secondary and tertiary structures determined by the far-UV and near-UV CD, and intrinsic tryptophan fluorescence (Fig. 2), the two proteins are nearly indistinguishable.

We also compared the total number of free thiol groups in the two proteins in their native as well as unfolded states in the presence of GuHCl, by using the DTNB assay. The number of accessible thiol groups in the folded native state were determined to be 3.91 ± 0.05 and 3.97

± 0.05 for MGB and S10R respectively, using a molar absorption coefficient of TNB^{2-} at 412 nm of 14,150 M^{-1} cm^{-1} (Fig. 3A). In the unfolded state, the number of accessible thiol groups were estimated to be 6.92 ± 0.05 and 6.98 ± 0.05 for MGB and S10R respectively using a molar absorption coefficient of TNB^{2-} at 412 nm of 13,700 M^{-1} cm^{-1} in solutions of buffered GuHCl (Fig. 3B)[7]. The theoretical number of cysteines in each protein is 9. Therefore, the DTNB assay estimates a shortfall of 2 sulfhydryls for both proteins in the unfolded state. However, both proteins have an equal number of free thiol groups in the folded as well as unfolded states.

At higher reaction times with DTNB (around 50–60 min), we noticed (Fig. 3C), that at 412 nm both proteins showed some precipitation which suggested possible protein aggregation and prompted us to monitor the absorbance also at 600 nm (Fig. 3D). Surprisingly, we found that the DTNB-treated solution of the mutant protein showed a higher rate of light scattering at 600 nm relative to the wild-type after an initial lag period, even though both proteins were estimated to have the same number of free thiol groups. Therefore, these aggregation profiles at 600 nm suggested a possible, thiol-based oxidation and aggregation behavior in *both* proteins - but with a clear difference in their aggregation profiles. The mutant protein aggregates at a significantly higher rate. We note here that while DTNB, or Ellman's Reagent, is generally used for the quantification of the number or concentration of free protein thiol groups[16], it is also a known "oxidizing agent" which preferentially oxidizes cysteine, leading to the formation of either protein disulfide bonds or mixed disulfides between protein and thiobenzoate[17,18]. Thus, our data are suggestive of cysteine oxidation-mediated protein aggregation.

To confirm whether the observed aggregation did in fact involve the oxidation of Cys residues, we examined the protein solutions at 60 min in Fig. 3C, using SDS-PAGE in the absence (Fig. 4A), and presence (Fig. 4B), of the reducing agent, β–mercaptoethanol. Fig. 4A clearly shows that the DTNB-reacted wild-type protein aggregates to form dimers both in the supernatant (lane 2), and more prominently in the pellet (lane 3). In contrast, the S10R mutant shows not only dimers but a series of higher molecular weight aggregates (lane 6) – with these aggregates being found predominantly in the pellet. Interestingly, the dimers in MGB and the aggregate "ladder" in S10R, both appear to be almost completely reducible to the monomeric state (Fig. 4B). These data thus strengthen our view that the observed protein aggregation is mediated by the oxidation of cysteine residues in both proteins, although the rate and extent of oxidation-mediated aggregation is significantly enhanced in the cataract-associated S10R mutant.

These findings were highly intriguing in light of the fact that the Ser to Arg mutation has no *direct i*nvolvement of Cys residues. However, we also questioned whether the findings could be an anomaly of the reaction of a non-biological oxidant such as DTNB with the proteins. To address this issue, we reacted both proteins with two biologically relevant oxidants (hydrogen peroxide and glutathione), as well as a second non-biological oxidant, diamide, which was included for additional confirmation of the oxidation-mediated effects (Fig. 5C). Diamide is also commonly used as a thiol-specific reagent in cell biology[19]. These data are shown in Fig. 5A, B & C.

3.2 Oxidation with H_2O_2

Fig. 5A shows the effect of H_2O_2 on the light scattering profiles of MGB and S10R. When oxidized with H_2O_2, both proteins show increased light scattering at 360 nm, but scattering from the mutant is higher (red open circles) than that of MGB (black solid circles). S10R also shows a higher accumulation of insoluble protein aggregates (red open squares), and consequently, a lower concentration of soluble protein remaining in the supernatant relative to MGB (black solid squares). Thus, a pattern consistent with that due to DTNB emerges also with the biologically relevant oxidant, H_2O_2. After about 2 and 4 hrs of reaction with H_2O_2, the number of free thiols in both proteins was estimated using the DTNB assay. Both show a reduction of about 2 ± 0.5 free thiols after 2 hr, and 3 ± 0.5 free thiols after 4 hr of reaction relative to the controls (7 ± 0.5), at the start of the reaction (0 hr). It is thus evident that, S10R, upon oxidation with H_2O_2, shows a higher propensity to aggregate than MGB, although the loss of thiol groups in both proteins is comparable.

3.3 Oxidation with GSSG

Because glutathione plays a key role in redox processes in the lens, we selected oxidized glutathione (GSSG) as our next biological oxidizing agent (Fig. 5B). Not surprisingly, the trends observed with DTNB and H_2O_2 are maintained also with oxidized glutathione for both proteins with regard to light scattering as well as protein concentration in the supernatant (Fig. 5B). Reaction with GSSG leads to a more rapid aggregation of S10R relative to MGB, again as revealed by the greater increase in A_{360}. This is consistent with the larger drop in soluble protein concentration of S10R in the supernatant.

3.4 Oxidation with Diamide

Diamide has been used[20] to examine the reactive cysteine residues in human γD-crystallin. Therefore, this non-biological oxidant was a logical choice to examine the effect on MGB and S10R to determine if the trends observed thus far were maintained with diamide. Because diamide has a broad λ_{max} around 360 nm, the aggregation profile was monitored at 400 nm instead. As shown in Fig. 5C, the trends observed with the other three reagents are indeed maintained also with diamide – and are consistent with the aggregation behavior seen previously, although the difference in aggregation is smaller.

3.5 Cysteine oxidation is directly responsible for the protein aggregation

To confirm that the three oxidants, H_2O_2, GSSG and diamide directly affect the cysteine thiols, we performed an SDS-PAGE analysis in the absence and presence of the reducing agent dithiothreitol (DTT, Fig. 6). The data clearly show that the “ladder of aggregates” seen in the absence of DTT, are reduced to monomers in the presence of the reducing agent. Interestingly however, the distinction between MGB and S10R in the extent of aggregation was not so obvious on the SDS gel in Fig. 6, unlike in the A_{360}/A_{400} solution assays (Figs. 5A–C), where they are clearly visible.

3.6 Comparison of the effects of oxidants

Thus, it is apparent from the above data that all four oxidants - both biologically relevant and non-biological - lead to an increase in disulfide-crosslinked protein aggregates, evidenced

by the increase in light scattering around 360–400 nm. S10R consistently shows a higher magnitude of oxidation and higher yield of aggregates as well as enhanced light scattering relative to MGB. In comparing the results of oxidation by the two non-biological reagents, DTNB and diamide, it is apparent that oxidation with DTNB results in the largest magnitude of difference between the two proteins, while diamide shows the smallest change. This difference is likely to be a result of the disulfide in DTNB being relatively weak[21], which makes it a better oxidizing agent for protein thiols. The DTNB reaction with thiols is driven thermodynamically to completion (e.g., mixed disulfide formation for all available cysteines in the target protein), – making DTNB the first choice for quantifying protein thiols[7]. Diamide, by contrast, does not oxidize all available cysteine residues in proteins[22], and the reaction is not -SH-SS exchange based. We used diamide with MGB and S10R because it has been shown to oxidize human γD-crystallin leading to the formation of both *intra*- and *inter*-molecular disulfide bonds[20]. We suggest that this may also be the case here.

3.7.1 Structural model of the S10R mutant and generation of a hydrophobic patch on the protein surface—To date, the 3D structure of MGB is not known. Therefore, we modeled the structures of MGB (not shown) and S10R (Fig. 7) as detailed in Materials and Methods. We reviewed these models and found that Arg10 in the mutant could help create a contiguous hydrophobic patch (Fig. 8), using the color schemes for hydrophobic regions, and acidic and basic charged groups according to Hagemans et al.[14]. In the Discussion section, we suggest how the S10R mutation creates a contiguous hydrophobic patch on the protein surface that could facilitate aggregation and enhance membrane binding relative to MGB.

3.7.2 Bioinformatics analysis of the reactivities of cysteine residues—Using our structural models (Fig. 7), we calculated the reactivities of all 9 Cys residues in MGB and S10R using bioinformatics tools as stated in Materials and Methods (section 2.6). The results of our bioinformatics analysis are presented in Table–2 and discussed in section 4.1.

4. DISCUSSION

Biologically relevant oxidants:

Oxidation with GSSG and H_2O_2 are of direct relevance to lens biochemistry. Reduced glutathione (GSH), plays a protective role in the lens, and the binding of two or three GSH molecules to the Cys residues of bovine γB-crystallin (BGB) has been shown[23]. The effects of its oxidized form, GSSG, and H_2O_2 however, are just the opposite[24]. Thus, depletion of GSH, and accumulation of GSSG are associated with oxidation of lens proteins and cataract[25]. GSSG forms adducts oxidatively with the γ–crystallins leading to the formation of both *intra*- and *inter*-molecular disulfide crosslinks and protein aggregation. Such disulfide-crosslinked aggregation of the γ–crystallins can occur even as a result of aerial oxidation, as we showed previously in BGB[26], and suggested that Cys15 is most likely to be one of the several cysteines involved. Since MGB has an 89% sequence identity with BGB whose 3D x-ray crystal structure is known to a very high resolution [Pdb ID 4gcr], it is reasonable to expect that similar oxidation-mediated effects would prevail also in MGB.

Unlike GSSG, H_2O_2 is a non-specific oxidizing agent, and besides thiols, can potentially oxidize other amino acids[27]. There is some evidence that it mainly oxidizes thiols in crystallins[28]. However, irrespective of the mechanisms of oxidation, both H_2O_2 and GSSG eventually lead to oxidized crystallins which form protein aggregates. Under our experimental conditions, it is apparent from SDS-PAGE[§] analysis (Figs. 4 & 6) that protein aggregates formed by such oxidation are S-S linked and are clearly reducible to the monomeric form.

Oxidation of cysteine thiols in the lens proteins and their relationship to cataract formation was noted as early as the 1950s[29]. The γ–crystallins have a high thiol content, and these thiols, along with small molecule thiols such as GSH maintain a reducing environment in the lens nucleus[30], and perhaps in other cellular environments[19]. Such an environment is clearly crucial in preventing oxidative damage and nuclear cataract. A vivid example of its importance is apparent in the treatment of human patients with hyperbaric oxygen which leads to the development of distinct nuclear opacities, along with severely reduced levels of GSH in the lens nucleus[31,32].

MGB has one of the highest cysteine contents among the γ–crystallins, (9 out of a total of 174 residues), and also contains the C(15)XXC(18)[33], and a C(18)XXXC(22)[34] motifs. The former has been frequently cited as important in the redox functions of many proteins, and the latter has occasionally been invoked in defining such a function. Thus, it is reasonable to expect that the increasing oxidation of Cys thiols as we have observed in the S10R mutant, would compromise the reducing atmosphere in the lens nucleus[19], and be detrimental to maintaining the redox balance in the nucleus[35] and for nuclear transparency.

Our data clearly highlight how a missense mutation at a site not involving a Cys residue, can activate multiple Cys residues in the protein – even as the mutant protein is structurally indistinguishable from the wild type. To understand how individual Cys reactivities may be altered by the S10R mutation and render them susceptible to oxidation, we turned to bioinformatics tools. Since the 3D-structural information for MGB is not available, we modeled the structures of MGB and S10R (Fig. 7) and calculated the reactivities of all 9 Cys residues. The results of our bioinformatics analysis are presented in Table–2 (section 4.1).

4.1 Reactivity of cysteine residues: A bioinformatics-derived analysis

In general, the reactivities of cysteine residues in proteins depend on their solvent accessibilities and microenvironments. Typically, these microenvironments consist of H-bonding networks which establish the pK_a values of the thiol groups, and the local polar and/or hydrophobic environments which further influence individual pK_a values. Taking this into account, we have examined in detail whether the solvent accessibilities of individual Cys residues and/or their pK_a values are altered following the mutation of Ser10 in MGB

[§]We noticed that, in our SDS-PAGE runs, the oxidized protein monomers typically appear to have lower apparent molecular weights than the reduced proteins, and most bands are smeared rather than discrete. Such anomalously low protein bands on SDS-PAGE gels have been seen also in other proteins[36,37], especially those high in cysteine content like MGB. The common explanation is that *intra*molecular disulfide crosslinks lead to multiple conformations (thereby causing fuzziness or smearing), and an apparent, lower size leading to higher mobility[36,37]. The fact that these are multiple forms of the same protein is confirmed by their reduction to a single band when treated with a reducing agent (Figs 4 & 6).

(Table–2), even though the structural models, and experimental spectral signatures of the structures of MGB and S10R are nearly identical.

The solvent accessibilities and computed pK_a values of all nine Cys residues are listed in Table–2. Our models show that Cys32 and Cys78 are totally buried and Cys109 is almost fully buried in both proteins. Therefore, according to our criteria, they are not predicted to be involved in oxidation-mediated aggregation in either protein. Cys18 has comparable accessibility and pK_a values, and Cys 15 is fairly solvent-accessible, and also has comparable pK_a values in both proteins, and hence, their reactivities are expected to be comparable in MGB and S10R.

Cys22 is totally buried in the mutant, but fairly accessible in MGB (Sγ accessibility 14 $Å^2$), and their pK_a values are comparable. Thus, *based on accessibility values alone, Cys22 is likely to be slightly reactive in the wild type b*ut unreactive in the mutant. Cys130 is marginally accessible (accessibility 5.2 $Å^2$) in the wild-type relative to the mutant (accessibility 0.18 $Å^2$) but given that its pK_a is nearly 3 pH units higher than that in S10R, it cannot be activated in MGB. Therefore, despite its limited exposure in S10R, *the much lower* pK_a of Cys130 would render it far more reactive in the mutant. Interestingly, Cys 41 meets both criteria in S10R – i.e., higher solvent accessibility and a pK_a which is almost 2 pH units lower than in MGB. Thus, the combined effect of a lower pK_a and higher accessibility would make Cys41 more reactive in S10R than in MGB. Finally, Cys79, with a significantly higher solvent accessibility in S10R, is predicted to exhibit higher reactivity despite a comparable pK_a in the wild type.

We conclude that, the surface localized Cys 15 is reactive in both MGB and S10R. Cys 22 is likely to be more reactive in the wild-type due to its accessibility, and Cys 79 and Cys 130 would be more so in the mutant based on accessibility alone (Cys 79), and pK_a alone (Cys 130). However, Cys 41 stands out in the mutant because of the combined effects of its significantly lowered pK_a and enhanced accessibility. Overall, the active Cys residues in the wild type are predicted to be Cys 15 and 22, and those in the mutant are Cys15, 41, 79 and 130, by our bioinformatics analysis. We recognize that our analysis does not take into account protein structural fluctuations or dynamics, which is an important, additional component of reactivity. If such fluctuations enhance the exposure of Cys 130 in S10R, which already has a low pK_a, the combined effect will clearly enhance its reactivity and also the overall reactivity of the mutant protein. Because several servers currently provide pK_a values, the absolute numerical values obtained from them vary considerably, but the differences in pK_a values for individual cysteines in MGB and S10R are quite close. While we have mainly used the CPIPE server[11], we have also used the DelPhiPKa[12] and the H^{++} servers[13] to compare pK_a values. Thus, our bioinformatics analysis provides a plausible basis for cysteine activation and oxidation – even though as stated above – the mutation itself does not involve a Cys residue and the solution structures of the two proteins are nearly identical. Our bioinformatics analysis simply suggests how certain Cys residues may be rendered more reactive in the mutant relative to the wild type, based on their solvent accessibilities and microenvironments. A definitive identification of the Cys residues involved in disulfide formation is ongoing[38], and is beyond the scope of this report.

Our *in vitro* work only demonstrates the observed effects in a homogeneous solution of a single protein, but the concentration of protein thiols is significantly higher in the lens nucleus. In that milieu, the introduction of readily oxidizable Cys residues from S10R can lead to heterogeneous intermolecular disulfides (i.e., among different proteins). Aggregation of the γ–crystallins, due to intermolecular disulfides is well known, and has long been cited in the etiology of cataract[5,39,40]. Spurious intermolecular disulfides are also known to be involved in other diseases besides cataract[41,42].

4.2 | The S10R mutation generates a hydrophobic patch on the protein surface

The S10R mutation creates an arginine-pair motif (R^9R^{10}), similar to those found frequently in proteins, and believed to afford stability to protein structures[43]. These motifs are also known to create local hydrophobic patches that help the proteins to aggregate on cell-membrane surfaces[44]. The side chain of Arg residues consist of delocalized charged guanidinium head and an aliphatic hydrophobic tail, consisting of Cβ and Cγ atoms. While the interactions of the charged head group often result in unexpected hydrophobic interactions, the hydrophobic tails also contribute to such interactions, although they also - counterintuitively - appear to play a major role in preventing peptide and protein aggregation[45]. Notwithstanding the ambiguous and unpredictable behavior of arginine clusters in proteins, it is clear that when they helps create hydrophobic surface patches, they render the surface interactive, facilitating protein aggregation and membrane-binding[46], as discussed below.

We have tried to pictorially depict the putative hydrophobic patch due to the S10R mutation (Fig. 8) based on the color representation provided in Hagemans et al.,[14]. However, we recognize that to substantively define a hydrophobic patch one would need to take several other factors into account[46]. Fig. 8 clearly shows how the Arg10 side chain, inserted between Arg9, Asp8 and Gln12, completes a hydrophobic patch on the one hand, and on the other connects with another patch consisting of Phe6, Phe11, Glu61, and Arg36, and extends further to include Pro63 and Tyr62 (Fig. 8A & Table – 3). Introduction of Arg10 in the mutant leads to a much larger contiguous hydrophobic surface patch, with a potential to enhance protein aggregation and membrane binding observed by Li et al[1]. Such a contiguous patch is not realized in MGB (Fig. 8C, D). While this is one plausible mechanism to explain protein deposits along the cell membrane, alternative mechanisms may be operational – such as ionic and chemical interactions with the cell membrane that would facilitate binding of the aggregated mutant protein to the membrane.

We should state that, experimentally we did not find a significant increase in hydrophobicity in S10R relative to MGB as measured by ANS and bis-ANS binding (data not shown). However, such small local changes in surface hydrophobicity may be difficult to detect by this method.

4.3 Effect of the overexpression of Cx46

The Gong group[1,2] also showed that, to a large extent, overexpression of Cx46 restores lens transparency in the S10R mutant mice. A significant question – still outstanding – is how the overexpression of Cx46 restores transparency in the mutant mouse lens nucleus?

These authors have also shown that protein aggregation in the mutant mouse lens is accompanied by the depletion of Cx46 followed by the disruption of the membrane-cytoskeleton structure of inner fiber cells[1,47,48]. We suggest that as a result of the S10R mutation, the Cys-activation and oxidation-mediated protein aggregates bind to the fiber cell membrane via hydrophobic or other interactions and block the gap junction channels containing the connexins. Many of these[1,2] and similar effects following protein aggregation have been seen in other cases. For example, in the rat model of selenite cataract, insoluble protein aggregates were shown to correlate with the loss of cytoskeletal proteins[49]. Protein aggregates in the lens are also known to lead to the degradation of lens fiber cells[50].

Taken together these observations support our view that the primary event in cataract formation in the S10R mouse is oxidation-mediated protein aggregation, and that all other changes observed – such as the gradual disruption of lens microarchitecture[51] – are downstream events.

We now consider the question of how transparency is restored following the overexpression of Cx46. Since GSH is not produced in the lens nucleus, it must be transported through the epithelial cells and lens cortex, or through the vitreous humor[52]. The supply of GSH is critical to maintaining the reducing environment in the nucleus. The GSH concentration is 6 mM, for example, in the normal, young human lens, but decreases in aged or cataractous lenses[25,53,54]. It follows that depletion of GSH – possibly arising from the loss of its transport through the disrupted fiber cell contacts in the S10R mouse – would render the proteins more susceptible to oxidative stress.

It has been shown that Cx46, whether in the gap junctions[3] or in hemichannels[55] acts precisely to deliver GSH from the cortex to the nucleus. Therefore, it is reasonable to surmise that the excess supply of GSH to the nucleus generated by the overexpression of Cx46, would ameliorate the effect of cysteine oxidation and subsequent formation of light-scattering protein aggregates. We suggest that this in fact, may be the most important function of Cx46 in the lens – i.e., to maintain the essential, reducing environment in the nucleus by ensuring a steady influx of glutathione – the primary antioxidant in the lens. Our conclusions regarding the role of the overexpression of Cx46 are based on the findings of other laboratories.

As our data strongly point to a Cys-mediated oxidative insult mechanism for the nuclear cataract in the S10R mutant mouse, we can argue how this could relate to human age-onset cataract (ARC). With few exceptions[56,57], the various animal models of ARC currently available do not strictly resemble its progression, metabolite composition, or the phenotype[57]. Therefore, better animal models are needed to test intervention strategies to delay or prevent ARC[58] .The S10R mouse model meets two important criteria: 1) The lens nucleus is depleted in GSH, and 2) the opacity seems restricted to the nucleus. Since the lens opacity in these mice seems primarily due to a failure of the redox apparatus – as it appears from our findings *in vitro* – we suggest that these mice could very well serve as appropriate animal models for ARC in which oxidative insult is a dominant mechanism. These mice are currently available at JAX (The Jackson Laboratory, B6.A-*Crygb*^{S11R}/BocJ, Strain #:003838, RRID: IMSR_JAX:003838)).

5. CONCLUDING REMARKS

Our study provides a plausible mechanism and explanation for the two key findings of Gong and coworkers: (i) nuclear cataract due to the S10R mutation in a mouse γ–crystallin, and (ii) the restoration of lens transparency by the overexpression of connexin Cx46. The main result from our work is that the primary cataractous event due to the mutation is protein thiol activation and oxidation, followed by protein aggregation. Other downstream changes are likely to follow eventually. We propose that overexpression of Cx46 restores transparency by replenishing the supply of reduced glutathione, thereby restoring the redox balance in the nucleus. Furthermore, we suggest that the S10R mouse could serve as a viable animal model for human age-onset cataract in which oxidative stress is the dominant risk factor for nuclear cataract.

Supplementary Material

Refer to Web version on PubMed Central for supplementary material.

ACKNOWLEDGEMENTS

The molecular graphic in Fig. 7 was produced using UCSF Chimera, developed by the Resource for Biocomputing, Visualization, and Informatics at the University of California, San Francisco, with support from NIH P41-GM103311. Fig. 8 was generated using Pymol software: The PyMOL Molecular Graphics System, Version 2.0 Schrödinger, LLC.

FUNDING STATEMENT

This work was supported by a National Institutes of Health Grant No. EY010535 to J.P.

DATA AVAILABILITY STATEMENT

No additional source data are required. The article contains all available data for the article.

REFERENCES

1. Li L, Chang B, Cheng C, et al. Dense nuclear cataract caused by the gammaB-crystallin S11R point mutation. Investigative ophthalmology & visual science. 2008;49(1):304–309. [PubMed: 18172107]
2. Li L, Cheng C, Xia CH, White TW, Fletcher DA, Gong X. Connexin mediated cataract prevention in mice. PloS one. 2010;5(9).
3. Slavi N, Rubinos C, Li L, et al. Connexin 46 (cx46) gap junctions provide a pathway for the delivery of glutathione to the lens nucleus. The Journal of biological chemistry. 2014;289(47):32694–32702. [PubMed: 25294879]
4. Asherie N, Pande J, Pande A, et al. Enhanced crystallization of the Cys18 to Ser mutant of bovine γB crystallin. Journal of molecular biology. 2001;314(4):663–669. [PubMed: 11733987]
5. Pande A, Pande J, Asherie N, et al. Molecular basis of a progressive juvenile-onset hereditary cataract. Proceedings of the National Academy of Sciences of the United States of America. 2000;97(5):1993–1998. [PubMed: 10688888]
6. Broide ML, Berland CR, Pande J, Ogun OO, Benedek GB. Binary-liquid phase separation of lens protein solutions. Proceedings of the National Academy of Sciences of the United States of America. 1991;88(13):5660–5664. [PubMed: 2062844]
7. Riddles PW, Blakeley RL, Zerner B. Reassessment of Ellman's reagent. Methods in enzymology. 1983;91:49–60. [PubMed: 6855597]

8. Kelley LA, Mezulis S, Yates CM, Wass MN, Sternberg MJ. The Phyre2 web portal for protein modeling, prediction and analysis. Nat Protoc. 2015;10(6):845–858. [PubMed: 25950237]
9. Roy A, Kucukural A, Zhang Y. I-TASSER: a unified platform for automated protein structure and function prediction. Nat Protoc. 2010;5(4):725–738. [PubMed: 20360767]
10. 'NACCESS' Computer Program [computer program]. Department of Biochemistry & Molecular Biology, University College, London, UK1993.
11. Soylu I, Marino SM. Cpipe: a comprehensive computational platform for sequence and structure-based analyses of Cysteine residues. Bioinformatics. 2017;33(15):2395–2396. [PubMed: 28369166]
12. Wang L, Zhang M, Alexov E. DelPhiPKa web server: predicting pKa of proteins, RNAs and DNAs. Bioinformatics. 2016;32(4):614–615. [PubMed: 26515825]
13. Gordon JC, Myers JB, Folta T, Shoja V, Heath LS, Onufriev A. H++: a server for estimating pKas and adding missing hydrogens to macromolecules. Nucleic Acids Res. 2005;33(Web Server issue):W368–371. [PubMed: 15980491]
14. Hagemans D, van Belzen IA, Moran Luengo T, Rudiger SG. A script to highlight hydrophobicity and charge on protein surfaces. Front Mol Biosci. 2015;2:56. [PubMed: 26528483]
15. Ji F, Jung J, Gronenborn AM. Structural and biochemical characterization of the childhood cataract-associated R76S mutant of human gammaD-crystallin. Biochemistry. 2012;51(12):2588–2596. [PubMed: 22394327]
16. Ellman GL. Tissue sulfhydryl groups. Archives of biochemistry and biophysics. 1959;82(1):70–77. [PubMed: 13650640]
17. Li A, Segui J, Heinemann SH, Hoshi T. Oxidation regulates cloned neuronal voltage-dependent Ca2+ channels expressed in Xenopus oocytes. J Neurosci. 1998;18(17):6740–6747. [PubMed: 9712645]
18. Todorovic SM, Jevtovic-Todorovic V, Meyenburg A, et al. Redox modulation of T-type calcium channels in rat peripheral nociceptors. Neuron. 2001;31(1):75–85. [PubMed: 11498052]
19. Hansen RE, Roth D, Winther JR. Quantifying the global cellular thiol-disulfide status. Proceedings of the National Academy of Sciences of the United States of America. 2009;106(2):422–427. [PubMed: 19122143]
20. Ramkumar S, Fan X, Wang B, Yang S, Monnier VM. Reactive cysteine residues in the oxidative dimerization and Cu(2+) induced aggregation of human gammaD-crystallin: Implications for age-related cataract. Biochim Biophys Acta Mol Basis Dis. 2018;1864(11):3595–3604. [PubMed: 30251679]
21. Whitesides GM, Lilburn JE, Szajewski RP. Rates of thiol-disulfide interchange reactions between mono- and dithiols and Ellmans reagent. Journal of Organic Chemistry. 1977;42(2):332–338.
22. Kosower NS, Kosower EM. Diamide: an oxidant probe for thiols. Methods in enzymology. 1995;251:123–133. [PubMed: 7651192]
23. Slingsby C, Miller L. The reaction of glutathione with the eye-lens protein gamma-crystallin. Biochem J. 1985;230(1):143–150. [PubMed: 4052032]
24. Giblin FJ. Glutathione: a vital lens antioxidant. J Ocul Pharmacol Ther. 2000;16(2):121–135. [PubMed: 10803423]
25. Reddy VN. Glutathione and its function in the lens--an overview. Experimental eye research. 1990;50(6):771–778. [PubMed: 2197112]
26. Pande J, Lomakin A, Fine B, Ogun O, Sokolinski I, Benedek G. Oxidation of gamma II-crystallin solutions yields dimers with a high phase separation temperature. Proceedings of the National Academy of Sciences of the United States of America. 1995;92(4):1067–1071. [PubMed: 7862635]
27. Hanson SR, Chen AA, Smith JB, Lou MF. Thiolation of the gammaB-crystallins in intact bovine lens exposed to hydrogen peroxide. The Journal of biological chemistry. 1999;274(8):4735–4742. [PubMed: 9988710]
28. McNamara M, Augusteyn RC. The effects of hydrogen peroxide on lens proteins: a possible model for nuclear cataract. Experimental eye research. 1984;38(1):45–56. [PubMed: 6705843]
29. Dische Z, Zil H. Studies on the oxidation of cysteine to cystine in lens proteins during cataract formation. Am J Ophthalmol. 1951;34(5 2):104–113. [PubMed: 14829519]

30. Srikanthan D, Bateman OA, Purkiss AG, Slingsby C. Sulfur in human crystallins. Experimental eye research. 2004;79(6):823–831. [PubMed: 15642319]

31. Palmquist BM, Philipson B, Barr PO. Nuclear cataract and myopia during hyperbaric oxygen therapy. Br J Ophthalmol. 1984;68(2):113–117. [PubMed: 6691953]

32. Riedl P, Skiljic D, Arnell P, Wannholt R, Zetterberg M, Andersson Gronlund M. Myopic shift and lens turbidity following hyperbaric oxygen therapy - a prospective, longitudinal, observational cohort study. Acta Ophthalmol. 2019;97(6):596–602. [PubMed: 30690920]

33. Quan S, Schneider I, Pan J, Von Hacht A, Bardwell JC. The CXXC motif is more than a redox rheostat. The Journal of biological chemistry. 2007;282(39):28823–28833. [PubMed: 17675287]

34. Ishikawa Y, Bachinger HP. An additional function of the rough endoplasmic reticulum protein complex prolyl 3-hydroxylase 1.cartilage-associated protein.cyclophilin B: the CXXXC motif reveals disulfide isomerase activity in vitro. The Journal of biological chemistry. 2013;288(44):31437–31446. [PubMed: 24043621]

35. Lou MF. Redox regulation in the lens. Prog Retin Eye Res. 2003;22(5):657–682. [PubMed: 12892645]

36. Pitt-Rivers R, Impiombato FS. The binding of sodium dodecyl sulphate to various proteins. Biochem J. 1968;109(5):825–830. [PubMed: 4177067]

37. Dunker AK, Kenyon AJ. Mobility of sodium dodecyl sulphate - protein complexes. Biochem J. 1976;153(2):191–197. [PubMed: 1275884]

38. Hou W PhD Thesis: Missense mutations in the gamma crstallins and mechanisms of lens opacity: Chemistry Department, University at Albany, State University of New York; 2020.

39. Thorn DC, Grosas AB, Mabbitt PD, Ray NJ, Jackson CJ, Carver JA. The Structure and Stability of the Disulfide-Linked gammaS-Crystallin Dimer Provide Insight into Oxidation Products Associated with Lens Cataract Formation. Journal of molecular biology. 2019;431(3):483–497. [PubMed: 30552875]

40. Serebryany E, Yu S, Trauger SA, Budnik B, Shakhnovich EI. Dynamic disulfide exchange in a crystallin protein in the human eye lens promotes cataract-associated aggregation. The Journal of biological chemistry. 2018;293(46):17997–18009. [PubMed: 30242128]

41. Welker E, Wedemeyer WJ, Scheraga HA. A role for intermolecular disulfide bonds in prion diseases? Proceedings of the National Academy of Sciences of the United States of America. 2001;98(8):4334–4336. [PubMed: 11274354]

42. Medinas DB, Rozas P, Martinez Traub F, et al. Endoplasmic reticulum stress leads to accumulation of wild-type SOD1 aggregates associated with sporadic amyotrophic lateral sclerosis. Proceedings of the National Academy of Sciences of the United States of America. 2018;115(32):8209–8214. [PubMed: 30038021]

43. Zhang Z, Xu Z, Yang Z, et al. The stabilization effect of dielectric constant and acidic amino acids on arginine-arginine (Arg-Arg) pairings: database survey and computational studies. The journal of physical chemistry B. 2013;117(17):4827–4835. [PubMed: 23581492]

44. Vazdar M, Heyda J, Mason PE, et al. Arginine “Magic”: Guanidinium Like-Charge Ion Pairing from Aqueous Salts to Cell Penetrating Peptides. Acc Chem Res. 2018;51(6):1455–1464. [PubMed: 29799185]

45. Das U, Hariprasad G, Ethayathulla AS, et al. Inhibition of protein aggregation: supramolecular assemblies of arginine hold the key. PloS one. 2007;2(11):e1176. [PubMed: 18000547]

46. Rego NB, Xi E, Patel AJ. Identifying hydrophobic protein patches to inform protein interaction interfaces. Proceedings of the National Academy of Sciences of the United States of America. 2021;118(6).

47. Wang K, Cheng C, Li L, et al. GammaD-crystallin associated protein aggregation and lens fiber cell denucleation. Investigative ophthalmology & visual science. 2007;48(8):3719–3728. [PubMed: 17652744]

48. Berthoud VM, Ngezahayo A. Focus on lens connexins. BMC Cell Biol. 2017;18(Suppl 1):6. [PubMed: 28124626]

49. Matsushima H, David LL, Hiraoka T, Clark JI. Loss of cytoskeletal proteins and lens cell opacification in the selenite cataract model. Experimental eye research. 1997;64(3):387–395. [PubMed: 9196390]

50. Santhoshkumar P, Xie L, Raju M, Reneker L, Sharma KK. Lens crystallin modifications and cataract in transgenic mice overexpressing acylpeptide hydrolase. The Journal of biological chemistry. 2014;289(13):9039–9052. [PubMed: 24554718]
51. Shiels A, Hejtmancik JF. Biology of Inherited Cataracts and Opportunities for Treatment. Annu Rev Vis Sci. 2019;5:123–149. [PubMed: 31525139]
52. Fan X, Monnier VM, Whitson J. Lens glutathione homeostasis: Discrepancies and gaps in knowledge standing in the way of novel therapeutic approaches. Experimental eye research. 2017;156:103–111. [PubMed: 27373973]
53. Harding JJ. Free and protein-bound glutathione in normal and cataractous human lenses. Biochem J. 1970;117(5):957–960. [PubMed: 5451916]
54. Kamei A Glutathione levels of the human crystalline lens in aging and its antioxidant effect against the oxidation of lens proteins. Biological & Pharmaceutical Bulletin. 1993;16(9):870–875. [PubMed: 8268853]
55. Shi W, Riquelme MA, Gu S, Jiang JX. Connexin hemichannels mediate glutathione transport and protect lens fiber cells from oxidative stress. J Cell Sci. 2018;131(6).
56. Fan X, Liu X, Hao S, Wang B, Robinson ML, Monnier VM. The LEGSKO mouse: a mouse model of age-related nuclear cataract based on genetic suppression of lens glutathione synthesis. PloS one. 2012;7(11):e50832. [PubMed: 23226398]
57. Lim JC, Umapathy A, Donaldson PJ. Tools to fight the cataract epidemic: A review of experimental animal models that mimic age related nuclear cataract. Experimental eye research. 2016;145:432–443. [PubMed: 26391448]
58. Lim JC, Grey AC, Vaghefi E, Nye-Wood MG, Donaldson PJ. Hyperbaric oxygen as a model of lens aging in the bovine lens: The effects on lens biochemistry, physiology and optics. Experimental eye research. 2021;212:108790. [PubMed: 34648773]
59. Pettersen EF, Goddard TD, Huang CC, et al. UCSF Chimera--a visualization system for exploratory research and analysis. J Comput Chem. 2004;25(13):1605–1612. [PubMed: 15264254]

HIGHLIGHTS

- The Ser10 to Arg mutation in mouse γB-crystallin leads to the activation of Cys residues without significant conformational change in the protein
- Under oxidizing conditions, activated Cys residues form intermolecular disulfide-crosslinked protein aggregates and lead to further downstream effects
- This work suggests a plausible explanation for the restoration of lens transparency following overexpression of connexin Cx46

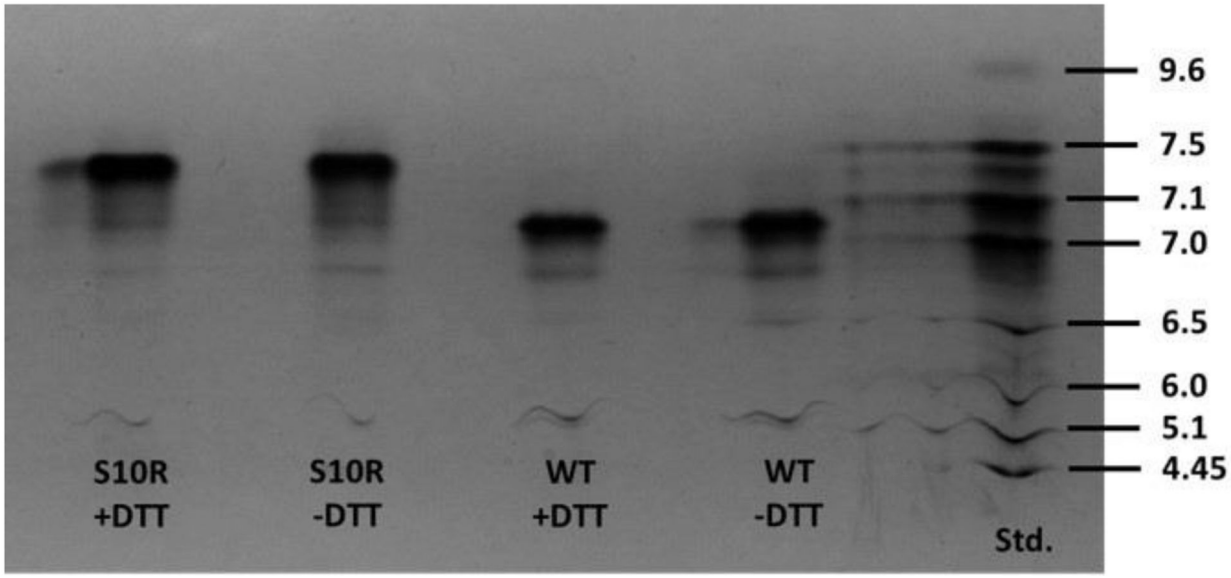

Fig. 1: A representative IEF gel showing the pI values of MGB and S10R.

pI values correspond to the prominent single bands on the IEF gel run in the presence of DTT. Based on three replicates of IEF, the pI values of MGB and S10R are estimated to be 7.05 ± 0.05 and 7.3 ± 0.1 respectively.

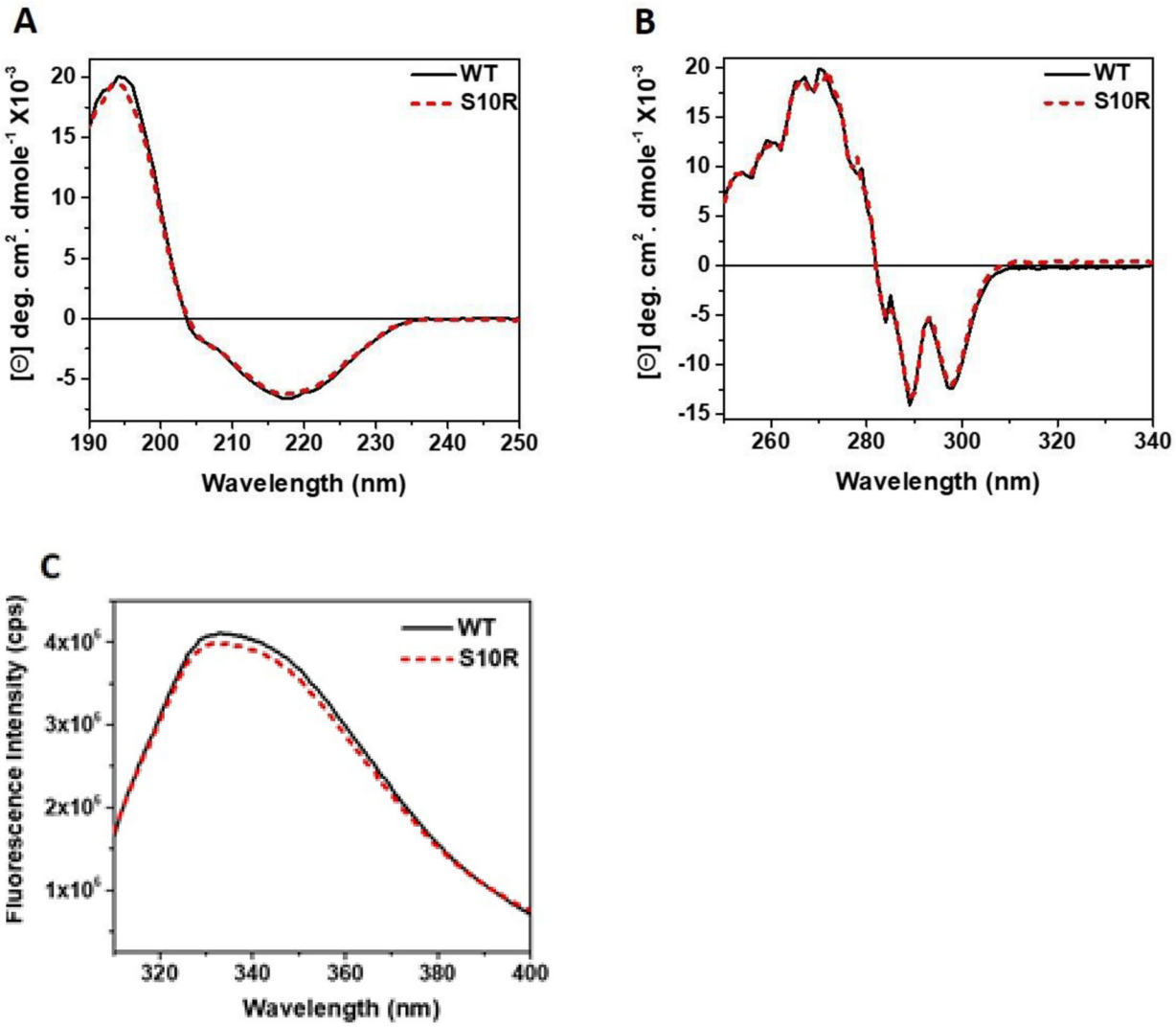

Fig. 2: Near and far-UV CD and fluorescence spectra of MGB and S10R

(A) Far-UV CD, protein concentration, 0.1 mg/mL in 10 mM phosphate buffer, pH 7.1, 1 mm path length, (B) Near-UV CD, protein concentration, 0.7 mg/mL in 100 mM phosphate buffer, pH 7.1, 10 mm path length. . Each CD spectrum is an average of 9 scans, (C) Tryptophan fluorescence spectra, protein concentration: 0.1 mg/mL in 10 mM phosphate buffer, pH 7.1, 3 mm pathlength.

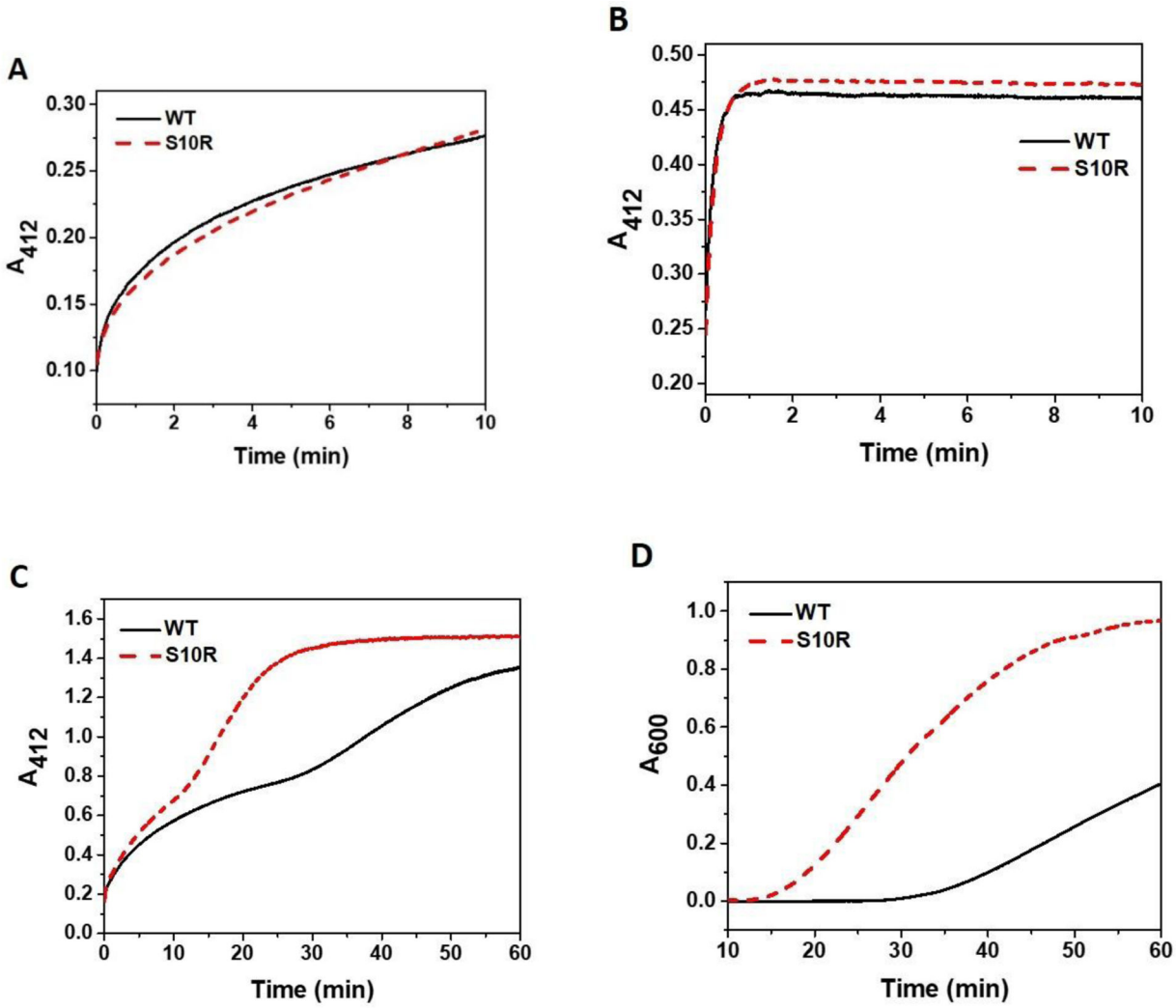

Figure 3: DTNB assay of WT and S10R.

(**A**) 0.1 mg/ml (5 μM) protein with 1 mM DTNB in mM phosphate buffer in the absence of GuHCl. (**B**) 0.1 mg/ml (5 μM) protein with 1 mM DTNB in mM phosphate buffer in the presence of GuHCl. (**C**) and (**D**) 0.2 mg/ml (10 μM) protein with 2 mM DTNB in mM phosphate buffer in the absence of GuHCl. Scattering at 412nm was first observed after the addition of 2 mM DTNB (**C**). Then scattering at 600 nm was measured as a function of time after the addition of DTNB (**D**). Each experiment was run in triplicate.

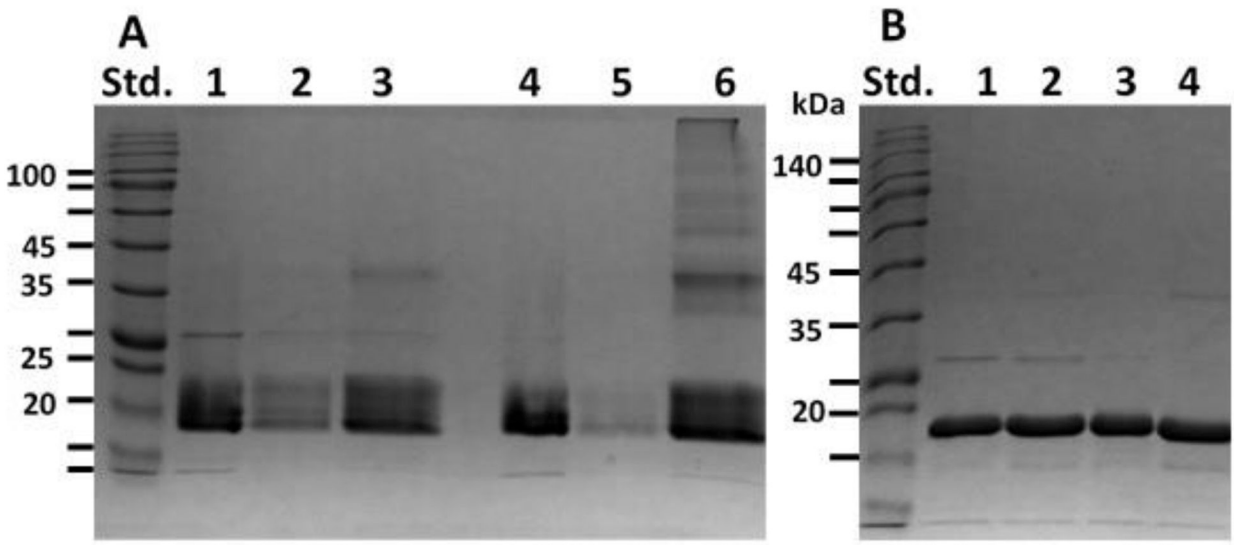

Figure 4: A representative SDS-PAGE of the DTNB-induced aggregation of proteins under (A) Nonreducing and (B) reducing conditions.

(A) Protein samples at 60 min time point from the DTNB assay were spun down and the supernatant and pellet were analyzed by SDS-PAGE in the absence of β-mercaptoethanol. Lane 1, MGB control; lane 2, MGB-DTNB supernatant; lane 3, MGB-DTNB pellet; lane 4, S10R control; lane 5, S10R-DTNB supernatant; lane 6, S10R-DTNB pellet (**B**) Protein samples at the end of the DTNB assay analyzed by SDS-PAGE in the presence of β-mercaptoethanol. Lane 1, MGB control; lane 2, MGB-DTNB product; lane 3, S10R control; lane 4, S10R-DTNB product.

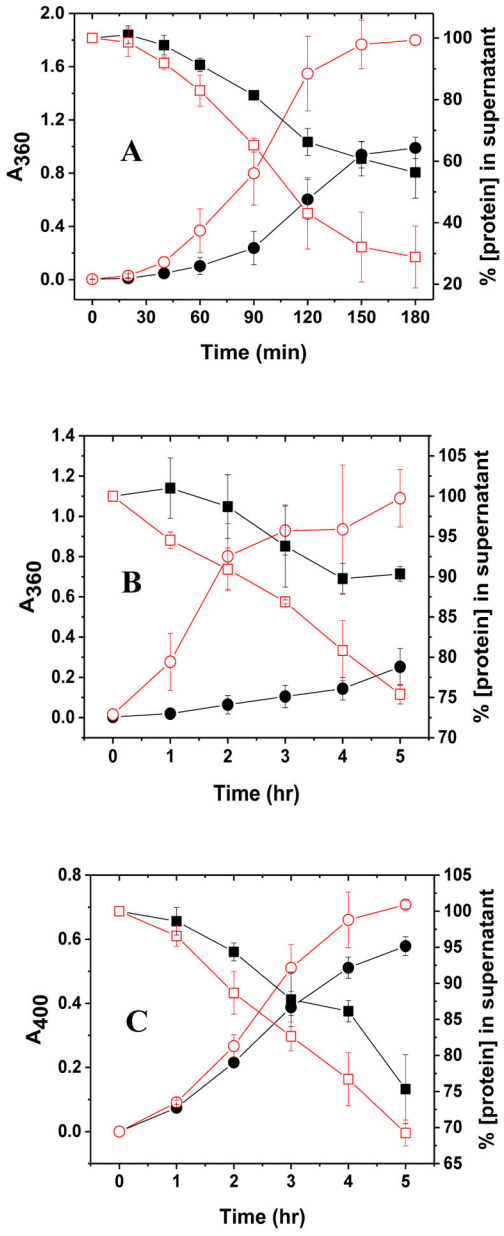

Figure 5: Effect of oxidizing agents on protein aggregation.

A) H_2O_2: 20 μM of each protein was incubated with 10 mM H_2O_2 in 100 mM Tris-HCl buffer, pH 8.5 at 37°C. Absorbance at 360 nm was measured as a function of time after the addition of oxidant. Samples withdrawn at different time intervals were spun down and protein concentration in the supernatant was measured. Data are the average of three experiments**. B) GSSG**: 20 μM of each protein was incubated with 15 mM GSSG in 100 mM Tris-HCl buffer (pH 8.5) at 37°C. A_{360} was measured as a function of time. Samples withdrawn at 1 hr intervals were spun down and protein concentration in the supernatant was measured. The supernatant was first dialyzed three times until the GSSG concentration was significantly lowered, and the last filtrate was used as a blank to measure A280 in the supernatant. Data are the average of three experiments. **C) Diamide**: 40 μM of each

protein was incubated with 1 mM diamide in 100 mM sodium phosphate buffer (pH 7.1) at 37°C. Absorbance at 400 nm was measured as a function of time after the addition of oxidant. Samples withdrawn at 1 hr intervals were spun down and protein concentration in the supernatant was measured. The supernatant was first dialyzed until the diamide concentration was less than 10 μM, and the last filtrate was used as a blank to measure A_{280} in the supernatant. Data are the average of two experiments. A), B), Solid circles, MGB (A_{360}); open circles, S10R (A_{360}); solid squares, MGB (% protein concentration in supernatant); open squares, S10R (% protein concentration in supernatant). C), Solid circles, MGB (A_{400}); open circles, S10R (A_{400}); solid squares, MGB (% protein concentration in supernatant); open squares, S10R (% protein concentration in supernatant).

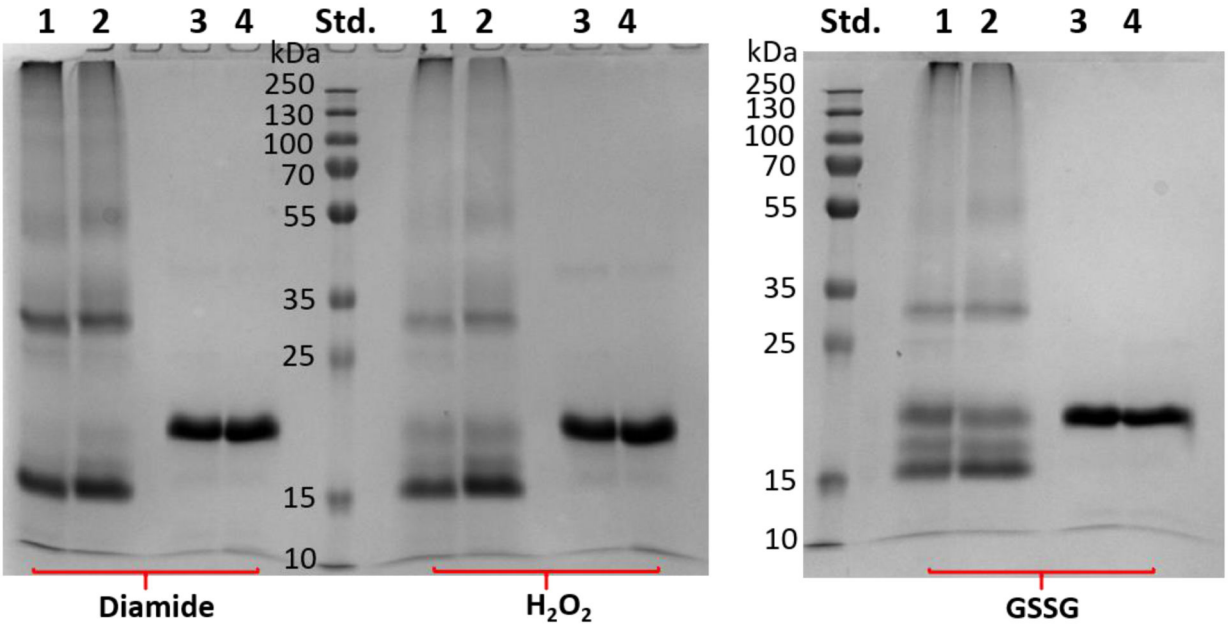

Figure 6: SDS-PAGE of MGB and S10R after reaction with the three oxidants, diamide, H_2O_2 and GSSG, in the absence and presence of DTT.

Following the reactions, whole samples were solubilized in 5% SDS and analyzed. Lane 1, MGB without DTT; lane 2, S10R without DTT; lane 3, MGB with DTT; lane 4, S10R with DTT.

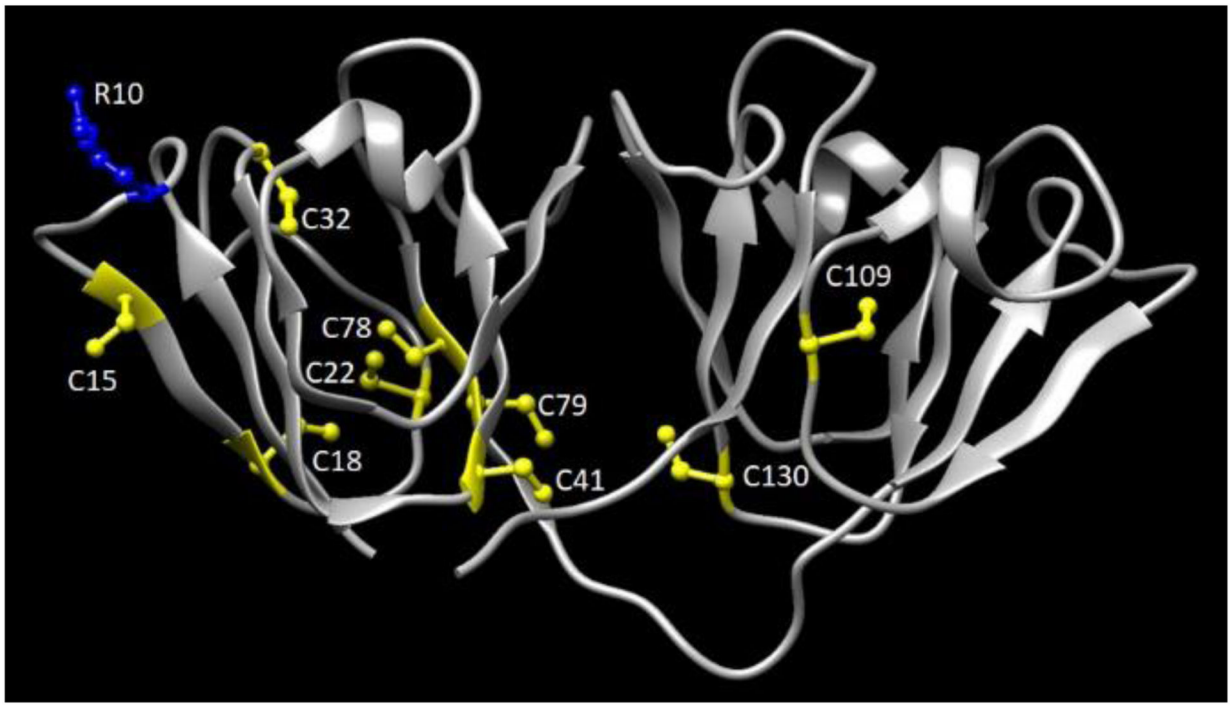

Fig. 7: Structural model of the S10R mutant.

Model shows the Cys residues in yellow and Arg10 in blue. Figure generated using the Chimera 1.13.1 software (Pettersen et al., 2004). (See Materials and Methods for additional details).

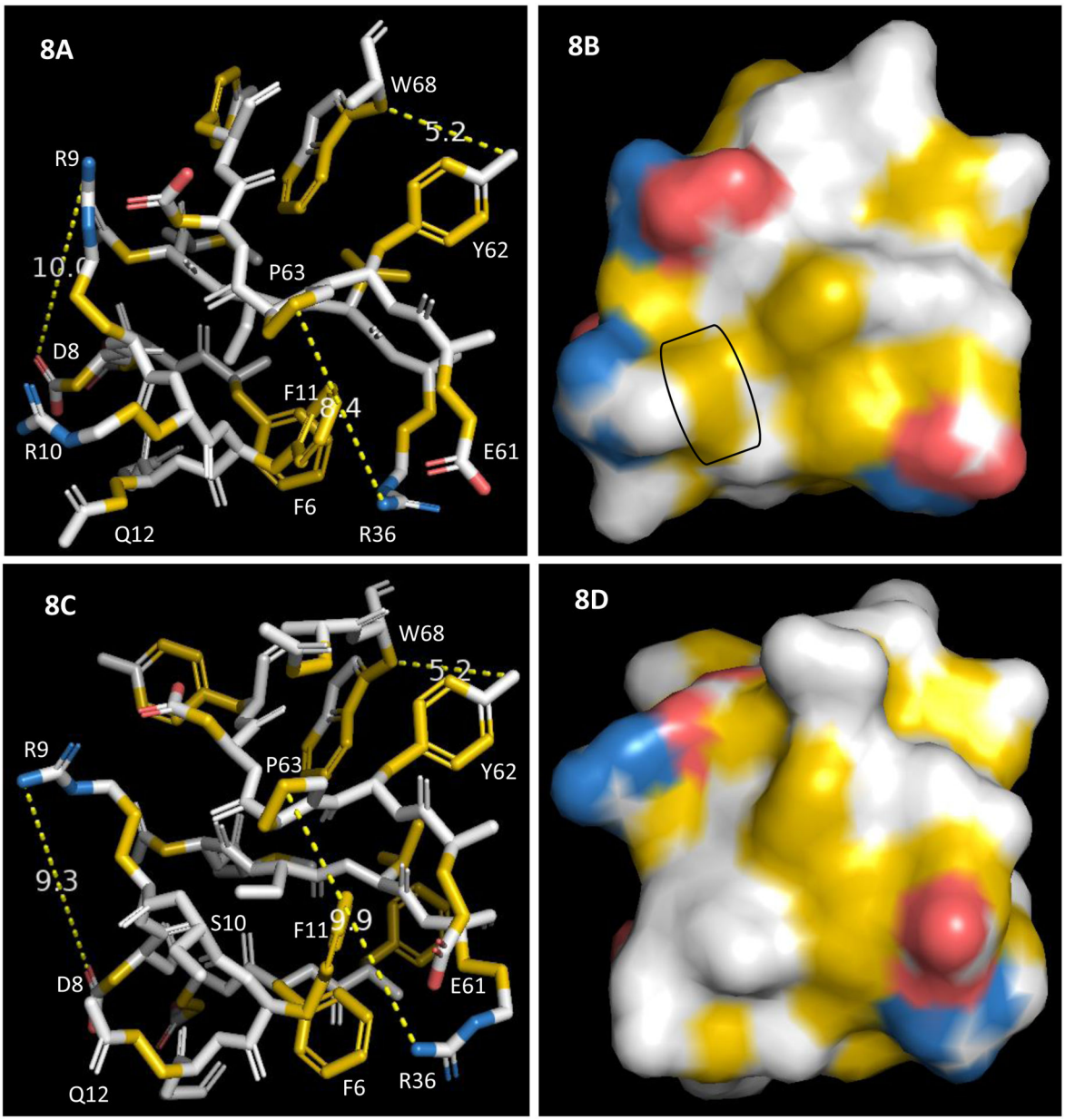

Figure 8:

(A): **Structural model of the S10R mutant**. A color-scheme denoting hydrophobic atoms as yellow, and positive and negative charges as blue and red respectively is used. Only residues within 10Å of the Cα of Arg10 are displayed. Hydrophobic atoms in Arg10 bridge those in Arg9, Asp8 and Gln12; they also connect the hydrophobic atoms of Phe6, Phe11, Arg36 and Glu61. *Thus, an almost contiguous hydrophobic patch consisting of these side chains, as well as those Trp67 and Tyr62 are created*. Dotted lines and numbers (in Å) represent distances between various atoms, as shown. **(B)** Surface representation of the structure of S10R in (A). Contribution of the side chain of Arg10 is shown as a black rectangle. **(C) Structural model of WT-MGB**. Only residues within 10Å of the Cα of Ser10 are shown in almost the same orientation as in (A) for comparison. **(D)** Surface

representation of the structure of MGB in (C). A comparison with (B) shows what we describe as a contiguous hydrophobic patch in (B), as opposed to distinct hydrophobic atoms intermingled with charged atoms here. The color schemes in Fig. 8 (A, B, C and D) are according to Hagemans et al[14]., "A script to highlight hydrophobicity and charge on protein surfaces", *Front Mol Biosci*. 2015;2:56. See main text for additional details.

Table - I

Protein Molecular Weights (MW) and molar extinction coefficients: MGB, mouse γB-crystallin, S10R, Ser10 to Arg mutant of MGB

Proteins	Theoretical MW (Da)	Experimental MW (Da)	Molar extinction coefficients (M^{-1} cm^{-1})
MGB	20,954.53	20,954.93 ± 0.05	44,350
S10R	21,023.63	21,024.22 ± 0.03	44,350

Table – II

Comparison of the Sγ accessibilities and pK_a values of Cys residues of MGB & S10R.

	MGB		S10R	
Residue no.	**Accessibility Sγ (Å^2)**	**pK_a**	**Accessibility Sγ (Å^2)**	**pK_a**
Cys15	48.82	8.34	51.14	8.74
§Cys18	3.76	6.97	3.03	6.66
§Cys22	13.96	7.23	0.00	7.58
§Cys32	0.00	6.58	0.0	6.60
Cys41	0.03	10.26	6.18	8.27
§Cys78	0.00	7.50	0.00	7.54
Cys79	1.68	10.29	17.95	10.16
Cys109	0.46	7.33	0.64	6.36
Cys130	5.19	8.45	0.18	5.15

Solvent accessibility of Sγ was determined using the NACCESS software and is expressed as (Å^2).

§pK_a values of Cys18, Cys22, Cys32 and Cys78 were determined using the DelPhiPK_a webserver. All other pK_a values were determined using the CPIPE webserver.

Table - III

Area of accessibility (Å^2) of exposed atoms of residues as shown in Fig. 8.A for S10R.

R9	Cβ (2.57), Cγ (23.30)
D8	Cβ (12.11)
R10	Cβ (10.36), Cγ (16.90)
Q12	Cβ (8.64), Cγ (11.71)
F6	CZ (9.11), CD2 (0.86), CE2 (14.60)
F11	Cβ (7.81), CD2 (8.78), CE2 (6.90), CZ (1.27)
R36	Cβ (3.42)
E61	Cβ (12.28), Cγ (13.40)
P63	Cβ (14.74), Cγ (37.86)
Y62	CD1 (0.03), CE1 (3.36), CD2 (0.10), CE2 (3.95)

Atomic accessibility was computed using NACCESS software (see main text), only non-zero values are shown. Residue R10 is highlighted. Its exposed hydrophobic atoms contribute ~27.3 Å^2 in surface area